Influence of Ge Composition in the $Cu_2Sn_{1-x}Ge_xS_3$ Thin-film Photovoltaic Absorber Prepared by Sulfurization of Laminated Metallic Precursor

Myo Than Htay[a,b,*], Takahiro Mandokoro[a], Hiroaki Seki[a], Takanori Sakaizawa[a], Noritaka Momose[d], Toshinori Taishi[c], Yoshio Hashimoto[a,b], Kentaro Ito[a]

[a]*Department of Electrical and Electronic Engineering, Faculty of Engineering, Shinshu University, Japan*
[b]*Institute of Carbon Science and Technology, Shinshu University, Japan*
[c]*Center for Energy and Environmental Science, Shinshu University, 4-17-1 Wakasato, Nagano 380-8553, Japan*
[d]*Department of Electrical and Electronic Engineering, National Institute of Technology, Nagano College, 716 Tokuma, Nagano 381-8550, Japan*

Abstract

$Cu_2Sn_{1-x}Ge_xS_3$ thin-film absorbers are prepared by sulfurization of laminated precursors. The crystal grain size is enhanced under higher growth temperature and/or sulfur pressure. By the XRD and Raman analyses, the crystal alloy is considered to be composed of majority monoclinic phase with minority secondary phase such as $Cu_2(Sn_{1-x}Ge_x)_3S_7$ throughout the whole Ge/(Ge+Sn) composition range. The optical band gap is observed to be varied between 0.94 eV and 1.30 eV in relation with the Ge contents. A photovoltaic conversion efficiency of about 2% is obtained in the sample utilizing $Cu_2Sn_{0.6}Ge_{0.4}S_3$ absorber.

Keywords: $Cu_2Sn_{1-x}Ge_xS_3$, Sulfurization, Thin film, Raman spectrum, Compound semiconductor, Solar cell
PACS: 78.30.Hv, 85.30.-z, 68.55.ag, 42.79.Ek, 88.40.hj

1. Introduction

Since the discovery of photovoltaic phenomenon in an asymmetrically illuminated electrodes pair in the early of 19th century by *Becquerel*, the conversion of solar energy directly into electrical energy by means of this phenomenon in the semiconductor materials is known to be one of the most attractive and efficient ways of solar energy harvesting [1, 2, 3, 4, 5, 6, 7]. In recent years, the photovoltaic efficiency of the thin-film solar cells based on a single junction of the compound semiconductors such as GaAs, $Cu(In,Ga)Se_2$, CdTe, and $Cu_2ZnSn(S,Se)_4$ are improving significantly [8, 9, 10, 11]. However, constrains on the resources of rare earth elements in the GaAs and $Cu(In,Ga)Se_2$ compounds, limitation due to the toxicity issue of CdTe, and the technical difficulties in the mass production of homogeneous $Cu_2ZnSn(S,Se)_4$ multinary compound are remained as the subjects to overcome. The search for new alternative compound semiconductor materials in the thin-film photovoltaic applications is still necessary to cope with the

*Corresponding author.Tel.: +81-(0)26-269-5241; fax: +81-(0)26-269-5220
Email address: myoth@shinshu-u.ac.jp (Myo Than Htay)

increasing commercial electrical energy demand. We previously reported that $Cu_2Sn_{1-x}Ge_xS_3$ ($0 \leq x \leq 1$) (CTGS) could be a potential alternative thin-film absorber material since it has absorption coefficient greater than 10^4 cm^{-1} order and it is possible to adjust its band gap to match with the solar spectrum range by controlling the Ge content of the alloy [12]. In addition to this properties, this material has an advantage on the environmental pollution issue since it is chemically stable and has no highly toxic elements composed in it. However, the researches concerning with this CTGS alloy in the thin-film photovoltaic applications are still in the early initial phase and the study on CTGS alloy itself with various Ge contents is still premature compared to the study of individual Cu_2SnS_3 (CTS) or Cu_2GeS_3 (CGS) ternary compounds [13, 14, 15, 16, 17, 18, 19, 20, 21, 22, 23, 24, 25, 26, 27, 28, 29, 30, 31, 32]. Up to now, only a few reports about the photovoltaic devices based on the CTGS with various Ge contents have been made [12, 33, 34]. Recently, *Umehara et al.* achieved a conversion efficiency as high as 6% in the cell utilizing CTGS absorber with Ge/(Ge+Sn) ratio of $x = 0.17$ ($E_g = 1.02$ eV) prepared by an open tube sulfurization technique showing that this material has a good potential for further improvement by adjusting to an optimum band gap by alloying with Ge [33, 34]. Hence, a detail study on CTGS alloy over the whole Ge composition range is an important issue in order to realize high efficiency photovoltaic devices utilizing this alloy material in the future. In this paper, we focused on the material properties of CTGS thin-film absorber in relation to the Ge concentrations and various synthesis conditions for a closed tube sulfurization technique.

2. Experimental methods

The CTGS thin-film alloys were prepared by sulfurization of precursors composed of Ge, Sn, and Cu laminated layers in a closed tube, which were deposited on the Mo coated soda-lime glass (SLG) substrates. For evaluations such as resistivity and transmittance measurements, the samples were deposited directly on the SLG. The composition ratios of the films were controlled by adjusting the thickness ratios of the individual elements. The Cu/(Ge+Sn) ratio was adjusted near the stoichiometric value of 1.95 ($\mp$0.05) for all the samples utilized in analyzing the effect of Ge content. Two types of precursors having a total thickness of 500 nm with different laminated layers (six and nine layers) were used in the experiments for investigating the influence of precursor structure. The details of the preparation of precursors and the sulfurization technique were reported previously [35, 36]. Effects on the material properties due to the difference in the final Ge composition were investigated by utilizing analyses such as a scanning electron microscopy (FE-SEM, Hitachi, S-4100), an electron probe microanalysis (EPMA; Shimadzu EPMA-1610), an X-ray diffractometry (XRD, Rigaku, RINT-2200V/PCSV, Cu $K\alpha$ ray; $\lambda = 1.5418$ Å with a Bragg-Brentano $\theta - 2\theta$ geometry at 40 kV, 30 mA), a laser Raman spectrometry (COMET-3504, an excitation source of $\lambda = 532$ nm, a 1800 line mm^{-1} grating), an optical transmittance measurement (Spectrophotometer, Shimadzu UV-3100), a heat-probe conductivity measurement, and a four-probe resistivity measurement (Kyowa Riken, K89PS, tips gap: 1 mm). The photovoltaic characteristic measurements were carried out under irradiance of 1000 W/m^2 at AM 1.5 spectrum (Wacom, HX-504). External quantum efficiency was acquired by a lock-in amplifier (EG & G Princeton applied research, Model-5210) with a reference signal obtained from a standard Si photodiode (Hamamatsu, S-1337). In fabricating the photovoltaic cells, chemical bath deposited CdS films were used as the counter n-type material to achieve heterojunction with the CTGS absorber layers. For the top transparent electrode, In_2O_3 (resistivity $3 \times 10^{-4} \Omega \cdot$ cm) thin films were deposited on top of the CdS layer by RF magnetron sputtering of a non-doped target (purity 99.99%) under pure Ar ambient without heating the substrate.

3. Results and Discussion

The surface morphologies of the samples with Ge/(Ge+Sn) ratio of x = 0.4 prepared under various sulfurization temperatures, sulfur ambient pressures, and different laminated precursor structures are shown in Fig. 1(a) to 1(f). It can be seen that the size of the crystal grain enhances with growth temperature as shown in Fig. 1(a) to 1(c). A maximum grain size of about 1.0 μm is obtained in the sample prepared under 0.27 atm and 570°C as shown in Fig. 1(c), which is almost thrice the size of the sample grown at 0.27 atm and 550°C as shown in Fig. 1(a). Fig. 1(d) and 1(e) show the surfaces of the samples prepared at sulfur pressures of 0.4 and 0.54 atm respectively. It can be seen that relatively larger crystal grain size is obtained under higher pressures compare to that prepared at 0.27 atm as shown in Fig. 1(a). Addition to this, the formation of protrusion textures in nanometer scale on the surface of the grain is obvious when prepared at higher pressures. In Fig. 1(f), the morphology of the sample prepared by sulfurization of the precursor with nine layers lamination structure under 0.27 atm at 550°C is shown. By comparing this sample with the one utilizing six layers lamination precursor as shown in Fig. 1(a), a larger crystal grain is achieved. Since the thickness of each single layer in the precursor with nine layers lamination is much thinner than that of the six layers, homogeneity of reaction during sulfurization could be much easier so that the enhancement of the crystal grain is realized. There was no obvious change in the surface morphology between the samples with different Ge contents but the thin films become brittle, and the formation of cracks and pinholes is quite often due to the mismatch of thermo expansion coefficient with the substrates at higher Ge contents (x >0.4). From the results of surface morphology analysis, it can be said that the preparation conditions such as the growth temperature, the sulfurizaiton pressure, and the structure of precursor are considered to be the important factors influencing the quality of thin-film absorber.

The detailed structures of the XRD patterns of the samples with various Ge contents prepared under sulfur pressure of 0.27 atm at 550°C are shown in Fig. 2(a) to 2(c). By the shifting of XRD peaks, it is found that the crystal lattice is shrunk when the composition of Ge is increased. In Fig. 2(a), the shifting of a prominent diffraction peak from the 2θ diffraction angle of 28.43° to 29.30° is observed when Ge content is increased. According to the database of the International Centre for Diffraction Data (ICDD) as shown in Tab. 1, the peak at 28.43° observed in the sample with x = 0.0 could be assigned as diffraction form either the (-131) crystallographic plane of monoclinic crystal structure or the (111) plane of cubic crystal structure of CTS, and the peak at 29.30° found in the sample with x = 1.0 could be originated from either the (112) plane of tetragonal or the (-131) plane of monoclinic crystal structure of CGS. In the case of peaks observed in the range between 46.8° and 49.6° as shown in Fig. 2(b), a prominent peak observed at 47.26° in the sample with x = 0.0, i.e. CTS, is shifted and split toward 48.40° and 48.98° as x approach the value of 1.0, i.e., Sn is completely substituted by Ge to form CGS. The peak at 47.26° could be assigned as either the (-133) plane of monoclinic or the (220) plane of cubic crystal. For the peak located at 48.98° in the sample with x = 1.0, it is closely fit with the peak due to the (204) plane of tetragonal phase but the possibility of the diffraction due to the (-133) plane of monoclinic phase could not be excluded. The peak denoted as "γ" in Fig. 2(b) is appeared near 47.74° in the sample with x = 0.4, and it is observed to be shifted toward 48.40° in the sample with x = 1.0. This value is found to be close to the diffraction of either the (220) planes of tetragonal phase or cubic phase or the (202) plane of monoclinic phase. Fig. 2(c) shows the detailed structures of XRD pattern observed between 55.0° and 59.5°. The peak observed at 58.62° is belonged to the Mo substrate. A prominent peak shifted from 56.08° to 57.56° is confirmed. From the observed peak position, the origin of the peak at 56.08° in the sample with x = 0.0 is considered to be

Table 1: Comparison of the positions of the XRD peaks of CGS and CTS phases with three possible crystal structures (*T*: tetragonal, *C*: cubic, *M*: monoclinic). The values close to the experimental results are described in bold letters.

	CGS (x = 1.0)			CTS (x = 0.0)			
	ICDD	ICDD	ICDD	ICDD	ICDD	ICDD	Experiment
Miller	00-041-1035	03-065-5562	01-088-0827	01-089-4714	01-089-2877	01-070-6338	data
index	*T*	*C*	*M*	*T*	*C*	*M*	
	2θ (Degree)						
112	**29.26**	-	-	28.54	-	-	29.30 (x = 1.0)
111	-	29.06	-	-	**28.45**	-	-
-131	-	-	**29.18**	-	-	**28.41**	28.43 (x = 0.0)
220	**48.32**	**48.38**	-	-	**47.31**	-	48.40 (x = 1.0)
204	**48.96**	-	-	47.47	-	-	48.98 (x = 1.0)
060	-	-	48.20	-	-	-	-
202	-	-	**48.27**	-	-	-	-
-331	-	-	48.72	-	-	-	-
-133	-	-	**48.85**	-	-	**47.21**	47.26 (x = 0.0)
312	**57.52**	-	-	56.32	-	-	57.56 (x = 1.0)
311	-	57.43	-	-	**56.13**	-	-
331	-	-	57.38	-	-	-	-
133	-	-	**57.46**	-	-	-	-
-402	-	-	-	-	-	**56.07**	56.08 (x = 0.0)
116	**58.52**	-	-	-	-	-	58.56 (x = 1.0)
-333	-	-	58.34	-	-	-	-
-204	-	-	58.44	-	-	-	-

originated from either (-402) plane of monoclinic phase or (311) plane of cubic phase of CTS, and the peak at 57.56° in the sample with x = 1.0 could be diffracted form either (133) plane of monoclinic crystal or (312) plane of tetragonal crystal of CGS as shown in Tab. 1. Another weak peak indexed as "β" around 56.92° in the sample with x = 0.4 is split toward 58.56° in the sample with x = 1.0. This peak could be assigned as the diffraction from the (116) plane of tetragonal crystal. By considering all these results, it is obvious that the crystal structure of the sample with no Ge content exhibits strong features of either monoclinic or cubic characteristics, while that of the sample with no Sn content shows strong tetragonal aspects with some major identities of the monoclinic phase. Since these samples were prepared at the growth temperature less than 600°C, it is reasonable to consider that the formation of high temperature (higher than 775°C) cubic phase is not favor [19, 20]. For the samples with $0.19 \leq x \leq 0.83$, the crystal structure is not distinguishable between either monoclinic or tetragonal. In considering the amount of

broadening of the peaks, it is hard to discriminate the position of the peaks with separation of less than about 0.1° in the XRD analysis, and hence it is not enough to identify the difference between the monoclinic and the tetragonal crystal phases just by this result alone.

The Raman spectra of the samples with various Ge contents measured at room temperature are shown in Fig. 3. The positions of the peaks for each spectrum are also plotted in Fig. 4 with the same indexing symbols shown in the Fig. 3. For the sample with $x = 0.0$, two prominent peaks labeled as "•" at 290 cm^{-1} and as "○" at 350 cm^{-1} are observed. These peaks could be assigned as the vibrations due to the monoclinic crystal of CTS [20]. In considering for the case of cubic crystal of CTS, the prominent peaks were reported to be located near 303 and 355 cm^{-1}, which are not agreed to our result [21, 22, 23]. When Ge content is increased, shifting of these peaks toward higher vibration frequencies is observed. The amount of shift exhibits moderate linear proportionality to the Ge composition in the alloys. In addition, broadening of the peak width is also detected in the samples with higher Ge contents, which could be due to the degradation of crystalline quality of the alloys or due to the coexistence of phases with small variation of Ge contents. In the sample with $x = 0.83$, the intensity of the peak denoted as "○" becomes too weak compared with the peak shown as "•" and totally vanish at the sample with $x = 1.0$. This could be due to the weakening of this vibration mode in the Ge dominant crystal. *Neumann et al.* reported that the possible crystal structure of a single crystal of CGS to be a monoclinic structure by infrared spectrum analysis [30, 31]. The peak labeled as "•" is found to be located at 323 cm^{-1} in the sample with $x = 1.0$ (CGS). The origin of this peak could be attributed to the vibration of the bond due to the cation-anion pairs, especially the bond between Cu and S atoms in the lattice, since its intensity is distinct throughout all the samples without any dependence on the Ge and Sn composition. In contrast, the origin of the peak shown by "○" could be related to the vibration mode that incorporated Sn atom because its intensity is strongly correlated with the composition of Sn in the samples. The other weak peaks denoted as "△", "▽", "◇", and "⧫" near 218, 262, 311, and 370 cm^{-1} in the sample with $x = 0.0$ are reported to be due to the Cu-poor secondary phase such as $Cu_2Sn_3S_7$ [20, 24]. These peaks also exhibit shifting towards higher vibration frequencies. It is also observed that the intensity of the peaks labelled as "◇" and "⧫" is greatly intense when the composition of Ge is increased. In the sample with $x = 1.0$, the peak at 393 cm^{-1} denoted as "⧫" is detected as the most prominent one. According to this observation, it could be considered that these vibration modes are much more favour in the Ge dominant lattice rather than in the crystal phase with Sn majority. Hence, the vibration origin of this peak could be related to that of the vibration of the bond interacting with the Ge atom of the primary phase such as monoclinic. Another broad shoulder labeled as "▼" is also found near 400 cm^{-1} in the sample with $x = 0.18$, which is not observed in the sample with $x = 0.0$. The intensity of this peak is increased and it is shifted toward higher vibration frequencies when the content of Sn is decreased. This peak also seems to be related to the Ge content and hence the origin of this vibration mode could be attributed to the vibration incorporating the Ge atom. In detailed analyses on the slopes of the least square approximation of each peak shifting in the samples with various Ge compositions as shown in Fig. 4, it is found that well fitted linear slopes could be divided into two distinct groups. The peaks denoted as "•", "◇", "○", and "⧫" belong to the first group with larger slope (see thick dash-lines in Fig. 4), and the peaks labeled as "△", "▽", and "▼" are in the second group with smaller one (see thin dash-lines in Fig. 4) except some deviation of the peaks indexed as "△" and "▽" in the sample with $x = 0.0$. The difference in the amount of peak shifting could be due to the existence of two different groups of vibration modes originated from separate crystal phases or due to the result of anisotropic nature of the inter atomic bonding strength in these samples. Since the intensity of the peaks of the first

group is relatively intense than that of the second group, it is reasonable to assign the origin of the vibration modes of the first group to the majority phase and the second group with relatively weak intensity to the minority secondary phase. The formation of Cu-rich secondary phases was not observed by either the XRD or Raman analysis in our samples, since the Cu/(Ge+Sn) composition ratios of the samples shown in Fig. 3 were confirmed to be less than 1.95 by EPMA, thus only the formation of Cu-poor phase such as $Cu_2Sn_3S_7$ could be possible as the secondary phase in a limited amount in addition to the majority stoichiometric phase of the CTGS alloy. In comparing the whole spectra of all the samples shown in Fig. 3, it can be noted that there are some common features between the spectra although the location of the peaks are different throughout the whole Ge composition range. For the samples corresponding to the CTS ($x = 0.0$) and CGS ($x = 1.0$) phases, there are six peaks with similar aspect for each. For the samples with $0.18 \leq x \leq 0.83$, there are seven peaks with similar features which could be assigned to either peaks belonging to that of the CTS or CGS phases. According to this fact, it may be reasonable to think intuitively that the crystal structure of the CTGS alloy could be form in a similar crystal phase such as monoclinic throughout the whole range of the Ge/(Ge+Sn) composition ratio.

The results of optical band gap of the CTGS thin films with various Ge contents, which were evaluated from the optical transmittance measurement and the extrapolation of the $(\alpha h\nu)^2 vs.\ h\nu$ plot, are shown in Fig. 5. However, the data for the sample with Ge content of about $x = 0.8$ was not able to measure because of the difficulty in preparing continuous thin film directly on the SLG substrate, which has a large thermo expansion coefficient mismatch with the CTGS thin films. At Ge/(Ge+Sn) ratio of $x = 0.0$, the optical band gap is about 0.94 eV and is increased to about 1.30 eV when Sn is completely substituted by Ge (at $x = 1.0$). By fitting the measurement data, the bowing parameter is observed to be about 0.09. Depending on the preparation conditions, a large deviation of the optical band gap under the same Ge content is observed, especially in the case of $x = 0.4$. This could be due to the existence of different crystal phases in the samples. The Raman spectra of the samples with Ge/(Ge+Sn) ratio of $x = 0.4$ prepared at different temperatures under 0.27 atm sulfur pressure utilizing six layers lamination precursors are shown in Fig. 6. A prominent broad peak denoted as "$*$" near 333 cm^{-1}, which is close to the reported main peak position (336 cm^{-1}) of tetragonal phase, is observed in the sample prepared at 550°C [22, 23, 24, 37]. When the growth temperature is increased to 570°C, the intensity of this peak is weakened and almost disappeared. On the other hand, two distinct peaks denoted as "$\bullet$" and "$\circ$" around 300 and 350 cm^{-1} become prominent, which are similar to those observed in the sample with $x = 0.4$ prepared by sulfurization of nine layers lamination precursor under 0.27 atm at 550°C as shown in Fig. 3. A small shift of the peak near 333 cm^{-1} at higher temperature could be due to the effect of superposition of surrounding peaks originated from the monoclinic and tetragonal phases. This result indicates that the growth temperature and the structure of laminated precursor are critical factors for achieving a homogeneous phase. In other words, it could be considered that the conditions necessary for the formation of tetragonal and monoclinic phases are very close so that a mixture of these two phases could form easily.

The result of the electrical resistivity measurements of the samples with various Ge contents is shown in Fig. 7. It is found that the resistivity of the sample with $x = 1.0$ is about 10^5 times larger than that of the sample with $x = 0.0$. *Khanafer et al.* also reported that the resistivity of CTS was lower than $10^{-1}\ \Omega \cdot$ cm order and that of the CGS to be varied between 10^2 and $10^4\ \Omega \cdot$ cm orders [28]. The correlation of resistivity with Ge concentration is very poor and large fluctuation of values is observed throughout the whole Ge composition range. This fluctuation could be due to the coexistence of different crystal phases as well as unintended secondary phases in the samples. All the films with various Ge contents showed p-type conductivity by

the heat-probe measurements although *Khanafer et al.* reported for both CTS and CGS to be an n-type conductivity by the Hall effect measurement [28]. According to the possibility of forming both conductivity types, these materials and its alloy could be applied for the fabrication of homojunction devices in the future. The photovoltaic characteristics of the solar cells utilizing CTGS absorber layers with various Ge contents are shown in Fig. 8. The data obtained from the samples prepared by the precursors of six layers lamination are shown in "□" and that of the nine layers lamination are plotted in "•". Up to now, we are able to achieve highest photovoltaic conversion efficiency (η) of about 2% with a fill factor (*F.F*) of about 40%, an open-circuit voltage (V_{OC}) of about 287.5 mV, and a short-circuit current density (J_{SC}) of about 16.8 mA/cm^2 from the sample having Ge/(Ge+Sn) ratio of x = 0.4. The *J-V* curve and external quantum efficiency of this sample are shown in Fig. 9. The tendency of increasing of the V_{OC} in the samples with higher Ge contents is found as shown in Fig. 8(c) and the highest value of about 300 mV is obtained in the sample with x = 0.83, although there are a few exceptions in the samples prepared by six layers lamination. However, the *F.F* of all the cells is still under 50% as shown in Fig. 8(b). On the other hand, the decreasing of J_{SC} with increasing Ge content in the samples is observed as shown in Fig. 8(d). The highest J_{SC} of about 25 mA/cm^2 is obtained in the sample with x = 0.18. It is also found that the reproducibility of the samples prepared by nine layers lamination is superior to that of six layers lamination. This could be due to the formation of relatively homogeneous thin films in the samples with nine layers lamination. On the other hand, the fluctuation of PV characteristics in the samples prepared by six layers lamination are relatively high. This implies that utilization of the precursors with six layers lamination could be more favorable in the formation of defects, coexistence of different crystal phases, and/or localized variation of Ge composition in the alloy films, which could degrade the performance of the cells seriously. In addition, a distinct deterioration of photovoltaic characteristic in the samples with Ge content higher than x = 0.4 is mainly due to the brittleness of the CTGS thin-film absorbers, which caused difficulties in preparing a good quality cell. These results indicate that there are still potential for the improvement of the photovoltaic conversion efficiency in the cell utilizing CTGS thin-film absorbers with higher Ge content if the formation of continuous thin film with homogeneous crystal phase on an appropriate substrate is achieved.

4. Conclusions

Thin films of $Cu_2Sn_{1-x}Ge_xS_3$ were prepared by sulfurization of laminated metallic precursors. The surface morphology of the CTGS thin-film absorbers was influent by the preparation conditions such as the growth temperature, the sulfur pressure, and the structure of laminated precursor. Crystal grain as large as 1.0 μm in diameter was easy to obtain in the sample prepared under higher pressure and/or temperature with nine layers lamination precursor. High incorporation of Ge (x >0.4) in the thin-film alloy caused the formation of cracks and pinholes mainly due to the mismatch of thermo expansion coefficient with the substrate. The peak shifting due to the shrinkage of lattice size with respect to the Ge content in the alloys was detected in both the XRD and Raman analyses. By the XRD and Raman analyses, the crystal structure of the alloy was considered to be composed of majority monoclinic phase when prepared by sulfurization of nine layers lamination precursors. The existence of secondary phase such as $Cu_2(Sn_{1-x}Ge_x)_3S_7$ was identified by the Raman spectroscopy data. The coexistence of monoclinic and tetragonal structure was also observed by the Raman analysis when prepared at temperature lower than 570°C utilizing six layers lamination precursors. The formation of monoclinic phase was observed more often than that of the tetragonal phase when using nine layers lamination precursors. The

CTGS thin-film absorbers with optical band gap ranged from 0.94 eV to 1.30 eV were obtained by varying the Ge contents of the alloys. A large variation of resistivity was observed especially when the Ge content was between $0.18 \leq x \leq 0.73$. A photovoltaic conversion efficiency of about 2% was obtained in the sample utilizing the $Cu_2Sn_{0.6}Ge_{0.4}S_3$ absorber. Increasing (decreasing) of the open-circuit voltage (short-circuit current density) in the samples with higher Ge composition was observed.

5. Acknowledgements

The authors would like to thank Mr. Isamu Minemura for his great help in setting up the experimental equipments.

References

[1] A. E. Becquerel, Researches sur les effects de la radiation chimique de la lumière solaire au moyen des courants électriques, C. R. Acad. Sci., 9 (1839) 145.
[2] A. E. Becquerel, Mémoire sur les effets électriques produits sous ĺinfluence des rayons solaires, C. R. Acad. Sci., 9 (1839) 561.
[3] W. Hallwachs, Ueber den einfluss des lichtes auf electrostatisch geladene Körper, Ann. Physik und Chemie, 33 (1888) 301.
[4] H. Hertz, Ueber einen einfluss des ultravioletten lichtes auf die electrische entladung, Ann. Physik, 31 (1887) 983.
[5] A. W. Copeland, O. D. Black, A. B. Garrett, The photovoltaic effect, Chem. Rev., 31 (1942) 177.
[6] J. Zhao, A. Wang, M. A. Green, F. Ferrazza, Novel 19.8% efficient honeycomb textured multicrystalline and 24.4% monocrystalline silicon solar cells, Appl. Phys. Lett., 73 (1998) 1991.
[7] J. Zhao, A. Wang, M. A. Green, 24.5% efficiency silicon PERT cells on MCZ substrates and 24.7% efficiency PERL cells on FZ substrates, Prog. Photovolt., 7 (1999) 471.
[8] B. M. Kayes, H. Nie, R. Twist, S. G. Spruytte, F. Reinhardt, I. C. Kizilyalli, G. S. Higashi, 27.6% Conversion efficiency, a new record for single-junction solar cells under 1 sun illumination, Photovoltaic Specialists Conference (PVSC), 2011 37th IEEE, 978-1-4244-9965-6/11, doi: 10.1109/PVSC.2011.6185831.
[9] P. Jackson, D. Hariskos, E. Lotter, S. Paetel, R. Wuerz, R. Menner, W. Wischmann, M. Powalla, New world record efficiency for Cu(In,Ga)Se_2 thin-film solar cells beyond 20%, Prog. Photovolt: Res. Appl., 19 (2011) 894.
[10] M. A. Green, K. Emery, Y. Hishikawa, W. Warta, E. D. Dunlop, Solar cell efficiency tables (version 44), Prog. Photovolt: Res. Appl., 22 (2014) 701.
[11] W. Wang, M. T. Winkler, O. Gunawan, T. Gokmen, T. K. Todorov, Y. Zhu, D. B. Mitzi, Device characteristics of CZTSSe thin-film solar cells with 12.6% efficiency, Adv. Energy Mater., 4 (2014) 1301465. doi: 10.1002/aenm.201301465.
[12] T. Mandokoro, M. T. Htay, N. Momose, T. Taishi, Y. Hashimoto, K. Ito, Preparation of $Cu_2Sn_{1-x}Ge_xS_3$ thin-film alloys by sulfurization and their photovoltaic properties, The 4th International Symposium on Organic and Inorganic Electronic Materials and Related Nanotechnologies, P3-57 (2013).
[13] N. Aihara, H. Araki, A. Takeuchi, K. Jimbo, H. Katagiri, Fabrication of Cu_2SnS_3 thin films by sulfurization of evaporated Cu-Sn precursors for solar cells, Phys. Status Solidi C, 10 (2013) 1086.
[14] D. Tiwari, T. K. Chaudhuri, T. Shripathi, U. Deshpande, R. Rawat, Non-toxic, earth-abundant 2% efficient Cu_2SnS_3 solar cell based on tetragonal films direct-coated from single metal-organic precursor solution, Sol. Energy Mater. Sol. Cells, 113 (2013) 165.
[15] K. Chino, J. Koike, S. Eguchi, H. Araki, R. Nakamura, K. Jimbo, H. Katagiri, Cu_2SnS_3 thin films by sulfurization of Cu/Sn stacked precursors, Jpn. J. Appl. Phys., 51 (2012) 10NC35.
[16] J. Koike, K. Chino, N. Aihara, H. Araki, R. Nakamura, K. Jimbo, H. Katagiri, Cu_2SnS_3 thin-film solar cells from electroplated precursors, Jpn. J. Appl. Phys., 51 (2012) 10NC34.
[17] Q. Chen, X. Dou, Y. Ni, S. Cheng, S. Zhuang, Study and enhance the photovoltaic properties of narrow-bandgap Cu_2SnS_3 solar cell by p-n junction interface modification, J. Colloid Interface Science, 376 (2012) 327.
[18] D. M. Berg, R. Djemour, L. Gutay, G. Zoppi, S. Siebentritt, P. J. Dale, Thin film solar cells based on the ternary compound Cu_2SnS_3, Thin Solid Films, 520 (2012) 6291.
[19] S. Fiechter, M. Martinez, G. Schmidt, W. Henrion, Y. Tomm, Phase relations and optical properties of semiconducting ternary sulfides in the system Cu-Sn-S, J. Phys. Chem. Solids, 64 (2003) 1859.

[20] D. M. Berg, R. Djemour, L. Gütay, S. Siebentritt, P. J. Dale, X. Fontane, V. Izquierdo-Roca, A. Pérez-Rodriguez, Raman analysis of monoclinic Cu_2SnS_3 thin films, Appl. Phys. Lett., 100 (2012) 192103.
[21] L. L. Baranowski, P. Zawadzki, S. Christensen, D. Nordlund, S. Lany, A. C. Tamboli, L. Gedvilas, D. S. Ginley, W. Tumas, E. S. Toberer, A. Zakutayev, Control of doping in Cu_2SnS_3 through defects and alloying, Chem. Mater., 26 (2014) 4951.
[22] Z. Su, K. Sun, Z. Han, F. Liu, Y. Lai, J. Li, Y. Liu, Fabrication of ternary Cu-Sn-S sulfides by a modified successive ionic layer adsorption and reaction (SILAR) method, J. Mater. Chem., 22 (2012) 16346.
[23] P.A. Fernandes, P.M.P. Salomé, A. F. da Cunha, Study of ternary Cu_2SnS_3 and Cu_3SnS_4 thin films prepared by sulfurizing stacked metal precursors, J. Phys. D: Appl. Phys., 43 (2010) 215403.
[24] A.-J. Cheng, M. Manno, A. Khare, C. Leighton, S. A. Campbell, E. S. Aydil, Imaging and phase identification of Cu_2ZnSnS_4 thin films using confocal Raman spectroscopy, J. Vac. Sci. Technol. A, 29 (2011) 051203.
[25] P. A. Fernandes, P. M. P. Salomé, A. F. da Cunha, Cu_xSnS_{x+1} ($x = 2, 3$) thin films grown by sulfurization of metallic precursors deposited by dc magnetron sputtering, Phys. Status Solidi C, 7 (2010) 901.
[26] M. Onoda, X. Chen, A. Sato, H. Wada, Crystal structure and twinning of monoclinic Cu_2SnS_3, Mater. Res. Bull., 35 (2000) 1563.
[27] X. Chen, H. Wada, A. Sato, M. Mieno, Synthesis, electrical conductivity, and crystal structure of $Cu_4Sn_7S_{16}$ and structure refinement of Cu_2SnS_3, J. Solid State Chem., 139 (1998) 144.
[28] M. Khanafer, O. Gorochov, J. Rivet, Etude des proprietes electriques des phases: Cu_2GeS_3, Cu_2SnS_3, Cu_8GeS_6 et Cu_4SnS_4, Mater. Res. Bull., 9 (1974) 1543.
[29] L. M. de Chalbaud, G. D. de Delgado, J. M. Delgado, A. E. Mora, V. Sagredo, Synthesis and single-crystal structural study of Cu_2GeS_3, Mater. Res. Bull., 32 (1997) 1371.
[30] H. Neumann, V. Riede, N. Sharif, H. Sobotta, M. S. Omar, Infrared optical properties and crystal structure of Cu_2GeS_3, Cryst. Res. Technol., 24 (1989) 227.
[31] H. Neumann, V. Riede, N. Sharif, H. Sobotta, M. S. Omar, Infrared lattice vibrations and crystal structure of Cu_2GeS_3, J. Mater. Science Lett., 8 (1989) 1360.
[32] H. Araki, K. Chino, K. Kimura, N. Aihara, K. Jimbo, and H. Katagiri, Fabrication of Cu_2GeS_3-based thin film solar cells by sulfurization of Cu/Ge stacked precursors, J. J. Appl. Phys., 53 (2014) 05FW10.
[33] M. Umehara, Y. Takeda, T. Motohiro, T. Sakai, H. Awano, R. Maekawa, $Cu_2Sn_{1-x}Ge_xS_3$ ($x = 0.17$) thin-film solar cells with high conversion efficiency of 6.0%, Appl. Phys. Express, 6 (2013) 045501.
[34] M. Umehara, Y. Takeda, K. Oh-ishi, Y. Aoki, T. Motohiro, T. Sakai, R. Maekawa, Energy level diagram around Ge-rich grain boundaries in $Cu_2Sn_{1-x}Ge_xS_3$ (CTGS) thin-film solar cells, Sol. Energy Mater. Sol. Cells, 134 (2015) 1.
[35] N. Momose, M. T. Htay, T. Yudasaka, S. Igarashi, T. Seki, S. Iwano, Y. Hashimoto, K. Ito, Cu_2ZnSnS_4 thin film solar cells utilizing sulfurization of metallic precursor prepared by simultaneous sputtering of metal targets, Jpn. J. Appl. Phys., 50 (2011) 01BG09.
[36] M. T. Htay, Y. Hashimoto, N. Momose, K. Sasaki, H. Ishiguchi, S. Igarashi, K. Sakurai, K. Ito, A cadmium-free Cu_2ZnSnS_4/ZnO heterojunction solar cell prepared by practicable processes, Jpn. J. Appl. Phys. 50 (2011) 032301.
[37] P. A. Fernandes, P. M. P. Salomé, A. F. da Cunha, Study of polycrystalline Cu_2ZnSnS_4 films by Raman scattering, J. Alloys Compd., 509 (2011) 7600.

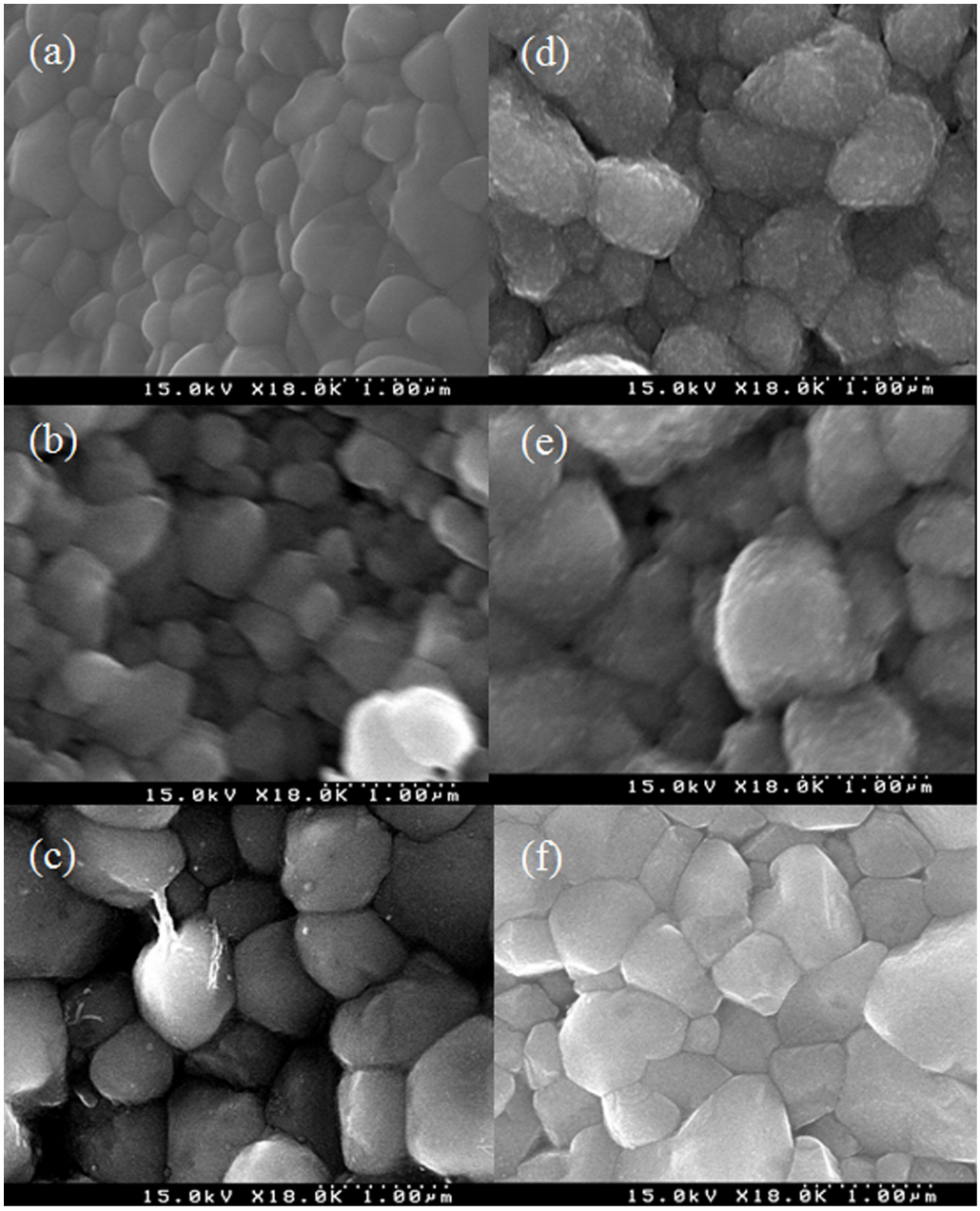

Figure 1: The surface morphologies of the samples with Ge/(Ge+Sn) ratio of x = 0.4 prepared at (a) 0.27 atm, 550°C, (b) 0.27 atm, 560°C, (c) 0.27 atm, 570°C, (d) 0.40 atm, 550°C, (e) 0.54 atm, 550°C for precursors with six laminated layers, and (f) 0.27 atm, 550°C for precursor with nine laminated layers.

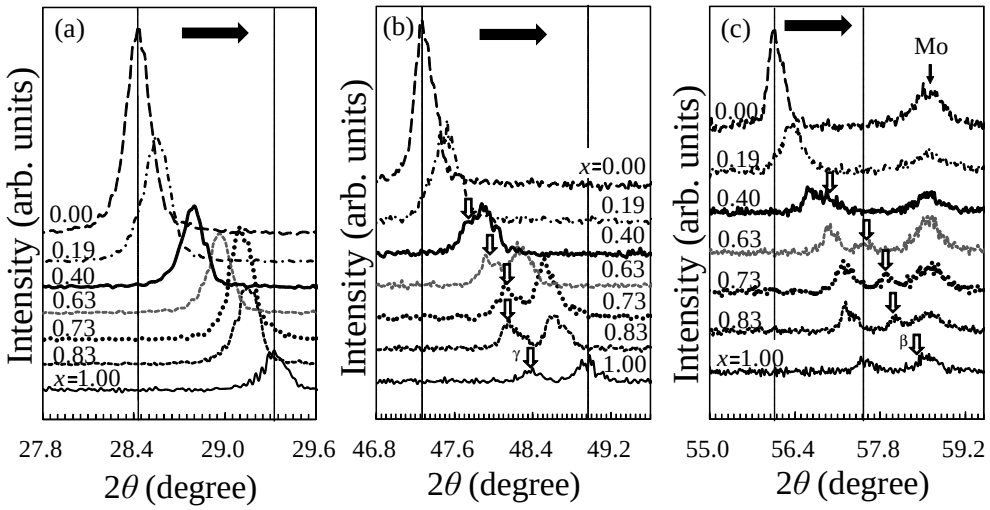

Figure 2: XRD patterns of the samples with various Ge contents showing the detailed structure of peaks at (a) 27.8° - 29.6° range, (b) 46.8° - 49.6° range, and (c) 55.0° - 59.5° range. Baseline offset is adjusted to enhance the visual of the spectra.

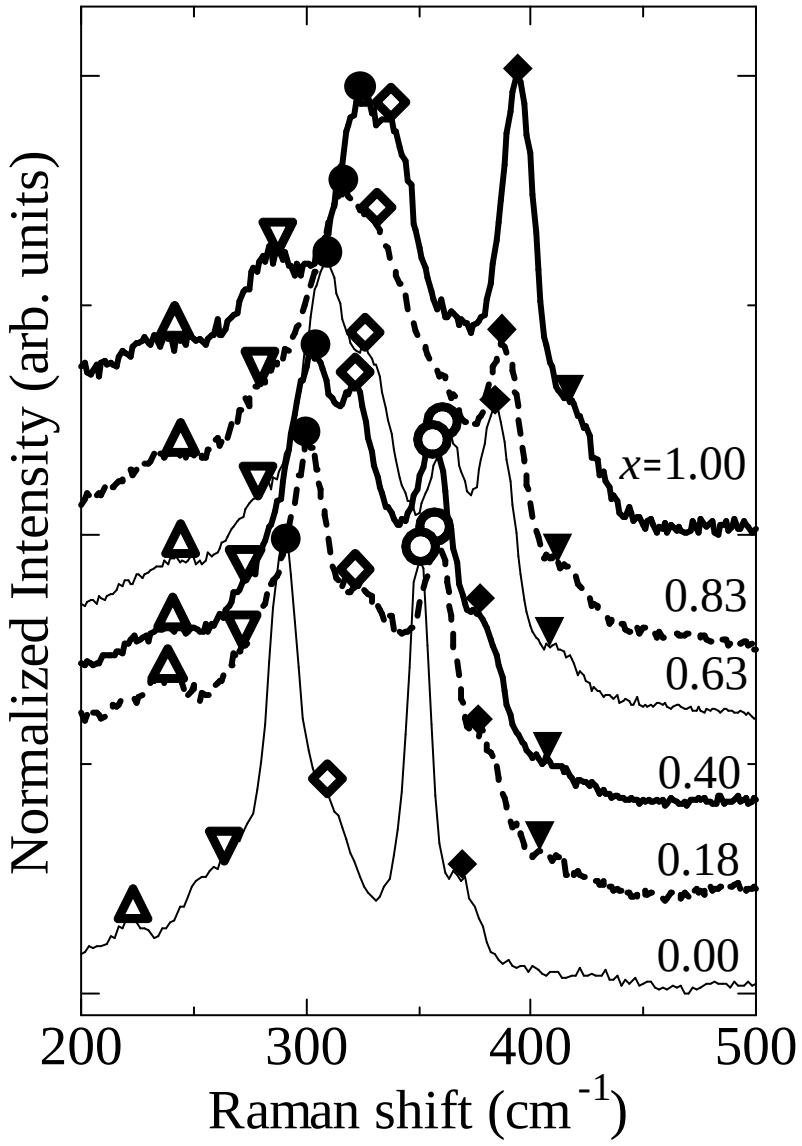

Figure 3: Raman spectra of the samples with various Ge contents measured at room temperature. The peaks denoted as "•", "◇", "○", and "♦" are assigned for the vibration modes due to the majority crystal phase. The peaks labeled as "△", "▽" and "▼" represent the vibrations due to the Cu-poor phase such as $Cu_2(Sn_{1-x}Ge_x)_3S_7$. All the spectra are normalized and the corresponding baseline offset is adjusted for visual enhancement.

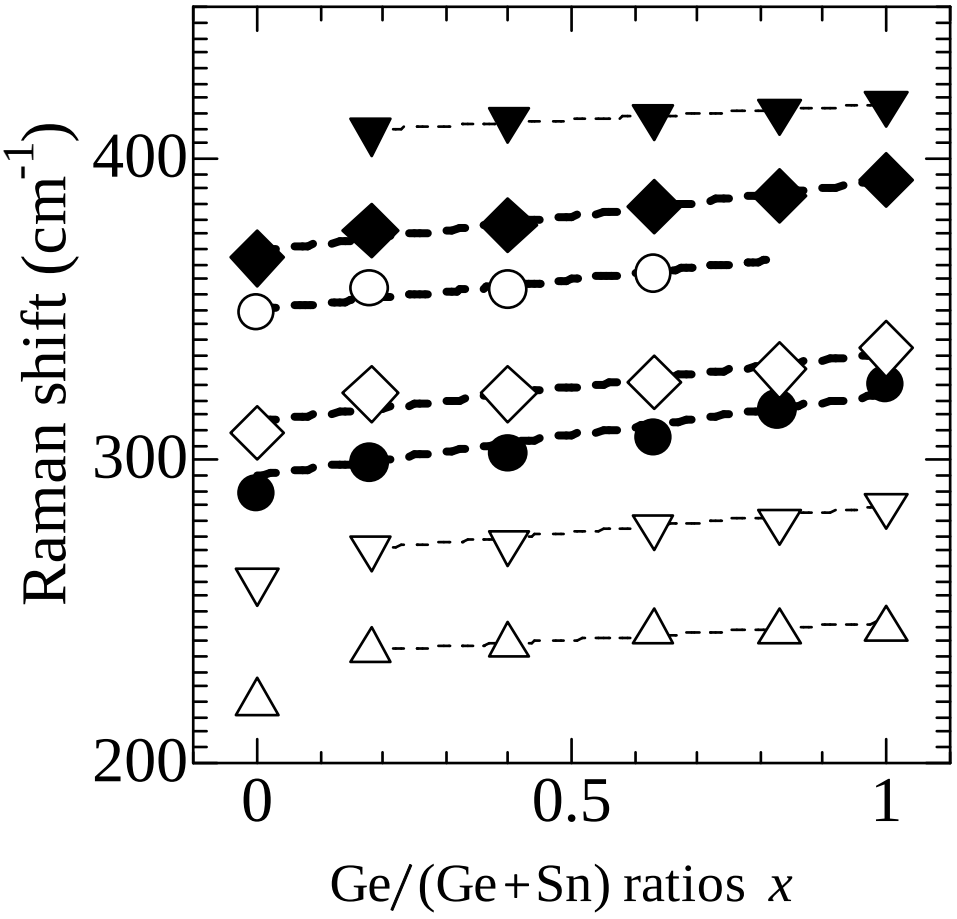

Figure 4: A graph showing the relationship of the position of the peaks of Raman shift with respect to the Ge contents in the CTGS alloys. The symbols plotted as "△", "▽", "•", "◊", "○", "♦", and "▼" are the positions of the corresponding peaks shown in Fig. 3 respectively. The dash-lines represent the least square approximation trends of the shifting. The thick dash-lines represent the peak shifting due to the majority phase, and the thin dash-lines show that of the Cu-poor minority phase.

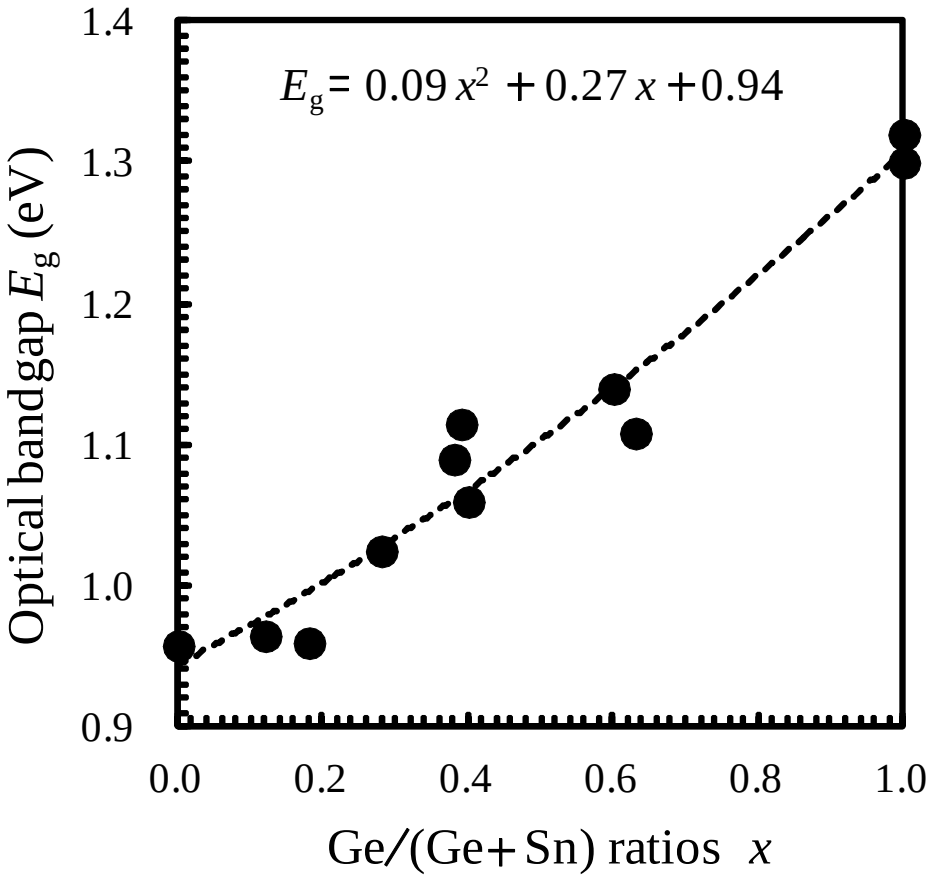

Figure 5: Variation of the optical bandgap with respect to the Ge content in the CTGS alloys.

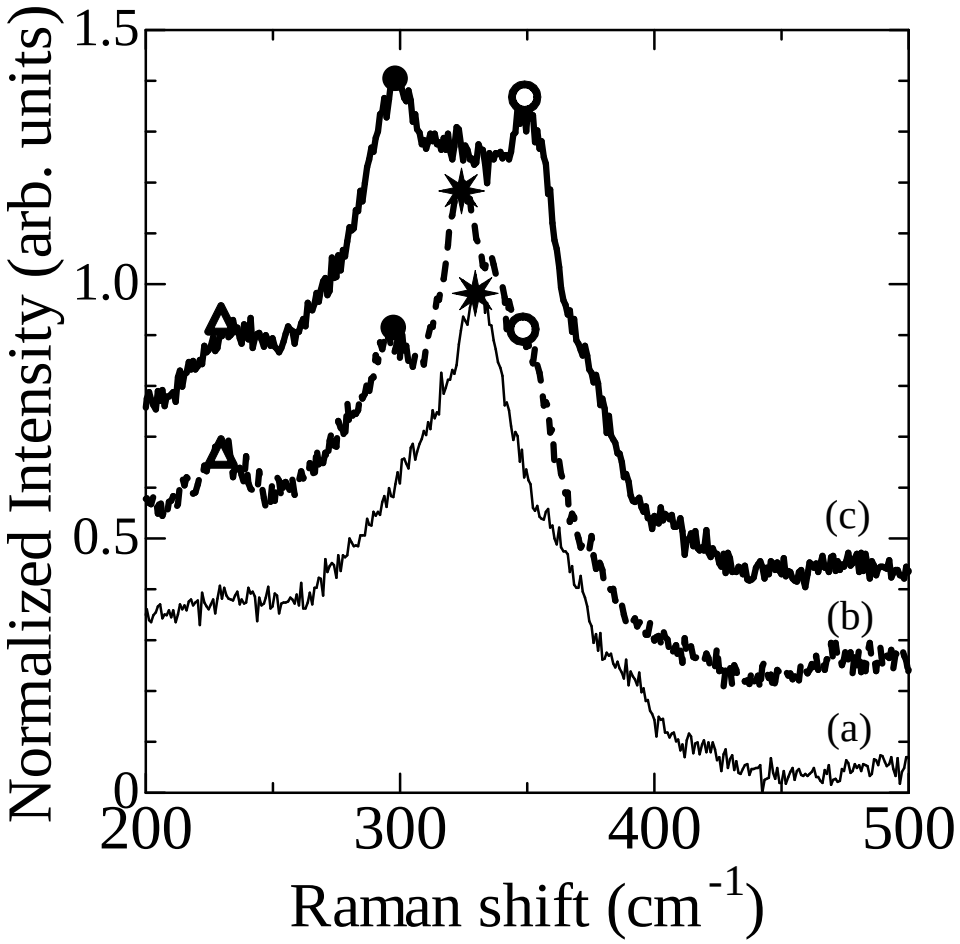

Figure 6: Raman spectra of the samples with Ge/(Ge+Sn) ratio of x = 0.4 prepared at different temperatures of (a) 550°C, (b) 560°C, and (c) 570°C utilizing precursors with six laminated layers. All the spectra are normalized with their most prominent peak observed in the 200-500 cm^{-1} range. The corresponding baseline offset is also made for visual enhancement.

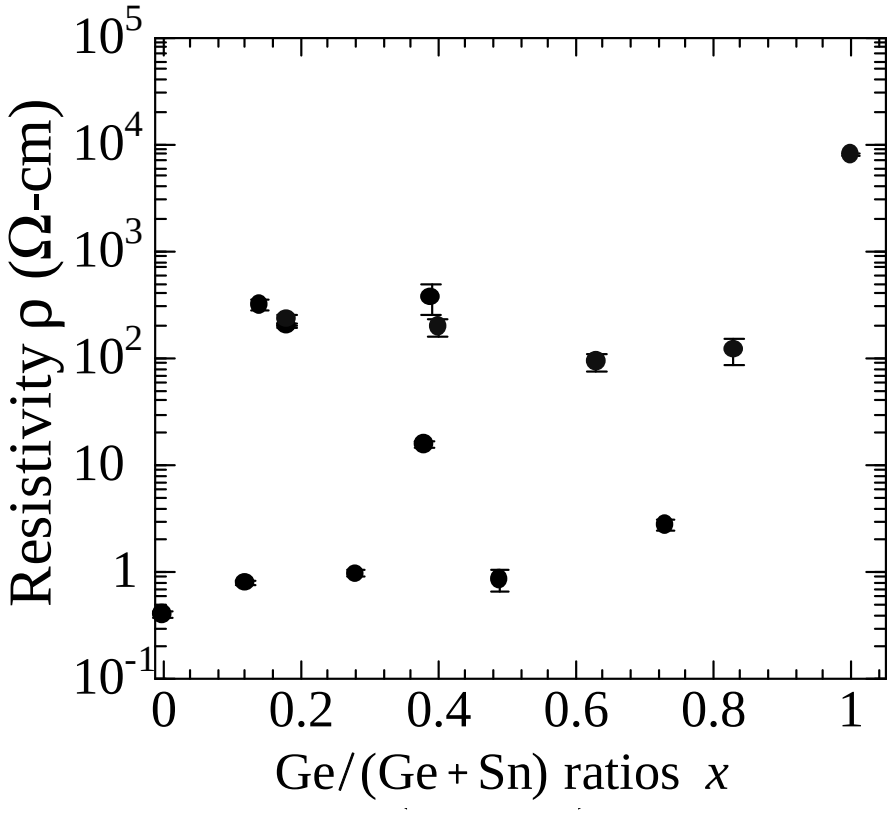

Figure 7: Variation of resistivity with respect to the Ge content in the CTGS alloys.

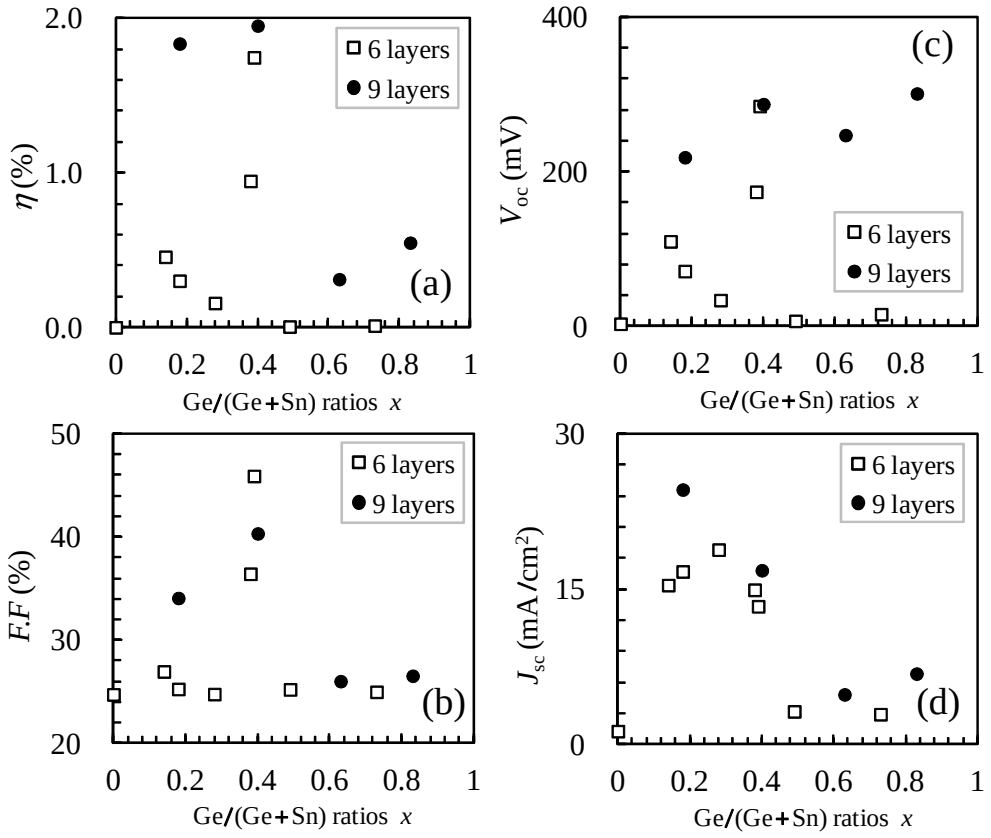

Figure 8: Variation of the photovoltaic characteristics with respect to the Ge content in the CTGS absorber layers: (a) conversion efficiency, η, (b) fill factor, *F.F*, (c) open-circuit voltage, V_{OC}, and (d) short-circuit current density, J_{SC}. Data plotted in filled circle (open square) were obtained from the samples prepared by nine (six) layers lamination precursors.

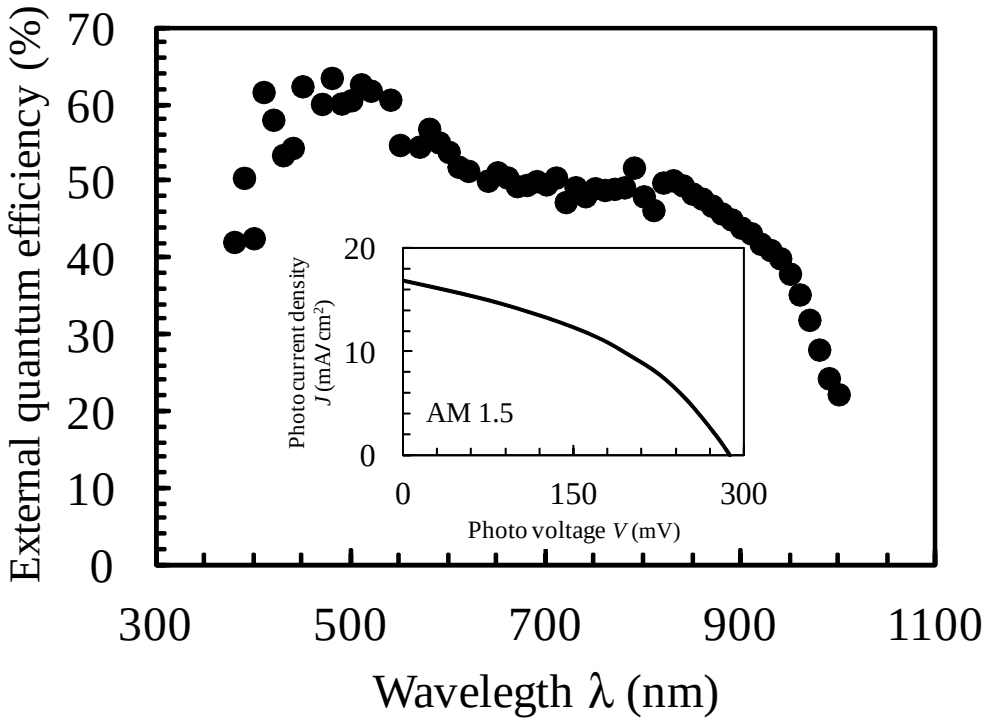

Figure 9: **The external quantum efficiency of the sample with Ge content of** $x = 0.4$ **prepared by the nine layers lamination precursor. The inset describes the corresponding *J-V* curve measured under illumination of 1000 W/m^2 (AM 1.5) at room temperature.**